BRIGHTNESS MEASUREMENTS OF THE ELSA ELECTRON BEAM

S. Joly, D.H. Dowell, J.P. de Brion, D.W. Feldman, G. Haouat, A. Loulergue and F. Schumann
Commissariat à l'Energie Atomique
B.P. 12, 91680 Bruyères-le-Châtel, France

Abstract

For high-power free-electron laser applications, an rf linac must deliver very bright electron beams. The ELSA linac has been designed to provide electron beams with low-emittance, high-peak current as well as low-energy spread ; these three quantities are of primary importance for getting high FEL performances. The electrons are produced by means of a photo-injector, accelerated by low-frequency rf cavities ; magnetic bunching at high energies is used to increase the peak current while minimizing the emittance growth. This paper presents recent measurements of transverse and longitudinal emittances of the electron beam for different bunch parameters.

Introduction

Many electron accelerator systems have recently been designed to produce high-peak current, low-emittance and low-energy spread bunches, especially for free-electron laser applications. Unfortunately, these goals are difficult to obtain simultaneously as, for example, the space charge forces due to high-peak currents increase both the transverse and the longitudinal emittances. However, these difficulties have been attenuated with the advent of photoelectric injectors which minimize the emittance growth. It is then possible to start with a fairly long pulse length, but limited by RF effects, and bunch the beam to the desired peak current after it reaches relativistic energy in a non-isochronous bend or transport system. This bunching occurs when a correct energy phase correlation is given to the electron bunch typically by dephasing the rf fields slightly from the maximum energy gain.

This paper reports on new longitudinal emittance measurements ; the technique has been described previously [1, 2] and will not be detailed here. These data will be combined with new transverse emittance measurements [3] leading to generalized brightnesses of the electron bunches.

All the measurements were made at a kinetic energy of 16.5 MeV. The injector exit energy was ~ 1.8 MeV with a - 30 degrees phase shift. Pulse duration was ~25 ps and the drive laser spot diameter on the photocathode was 4 mm.

Longitudinal emittance measurements

Analysis of the longitudinal emittance data

The emittance data for electron beam experiments are usually assumed to be described by an ellipse in the phase space plane. In the case of the longitudinal phase space, each electron's conjugate variables of energy and time are assumed to fall within the boundaries of an ellipse defined by

$$\gamma\Delta t^2 + 2\alpha\Delta t\Delta E + \beta\Delta E^2 = \frac{\varepsilon_l}{\pi} \qquad (1)$$

Here α, β and γ are the Twiss parameters for the longitudinal phase space ellipse and ε_l is the longitudinal emittance.

The longitudinal beam matrix τ is defined in terms of the Twiss parameters in a manner analogous to the transverse phase space ellipse, i.e.

$$\tau = \begin{pmatrix} \tau_{11} & \tau_{12} \\ \tau_{12} & \tau_{22} \end{pmatrix} = \varepsilon_l \begin{pmatrix} \beta & -\alpha \\ -\alpha & \gamma \end{pmatrix} \qquad (2)$$

In terms of the beam matrix elements, the pulse length is given by $\sqrt{\tau_{11}}$ and the energy spread by $\sqrt{\tau_{22}}$. The units of the τ-matrix have been chosen to be picoseconds (ps) and MeV. And for comparison with the experimental results, the pulse length and energy spread represent full width half maxima (fwhm).

In general, the analysis of transverse emittance data involves determining the beam matrix elements for the phase space ellipse. However, the longitudinal phase space is highly non-linear which means it cannot be represented by a simple phase space ellipse. Therefore, the approach taken here is to distort the ellipse with a power series.

Specifically, we begin with the ellipse defined by Eq. (1), solve for the energy spread and add quadratic and cubic terms to introduce the distortion. The ellipse boundary is then described by :

$$\Delta E = -\frac{\alpha}{\beta}\Delta t \pm \sqrt{\left(\frac{\alpha}{\beta}\Delta t\right)^2 - \frac{\gamma\Delta t^2 - \frac{\varepsilon_l}{\pi}}{\beta}} + a\Delta t^2 + b\Delta t^3 \qquad (3)$$

Our longitudinal data is then analysed to determine not only the three ellipse parameters but also the additional factors, a and b, at the exit of the injector cavity.

The experiment is performed by measuring the beam energy spread and pulse length distribution or the time spectrum of the beam at various 433 MHz accelerator RF phases. The accelerated beam energy and time spectra are measured after the non-isochronous bend. The data is analysed by assuming the following transformation of energy and time from the exit of the 144 MHz injector cavity to the entrance of the 180 degree bend, hereafter referred to as the demi-tour (see Fig. 1) :

$$\Delta E_1 = \Delta E_0 + E_{433}(\sin(\phi_{433} + \Delta t_0) - \sin(\phi_{433})) \qquad (4a)$$

$$\Delta t_1 = \Delta t_0 \qquad (4b)$$

Here ΔE_0 and Δt_0 are the electron's initial energy and time deviation from the central ray at the exit of the 144 MHz

injector cavity. E_{433} is the maximum energy gain for the 433 MHz cavities and $\varnothing_{433}$ is the phase of the central ray relative to the crest of the 433 MHz RF wave form. ΔE_1 and Δt_1 are the energy and phase after the accelerator and before the demi-tour.

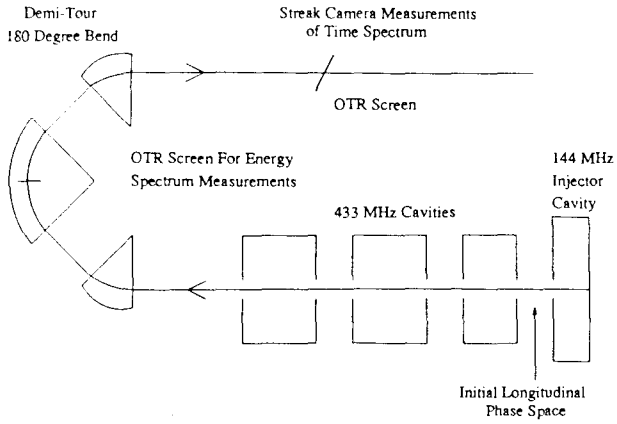

Fig. 1 Experimental layout of the ELSA accelerator for the longitudinal emittance measurements.

The temporal transformation in Eq. 4b assumes the beam is relativistic and no RF bunching is present. The transport around the demi-tour is given very simply in terms of the bend's non-isochronicity δ (with units of ps/MeV).

$$\Delta E_2 = \Delta E_1 \qquad (5a)$$

$$\Delta t_2 = \Delta t_1 + \delta \Delta E_1 \qquad (5b)$$

Where ΔE_2 and Δt_2 are the electron coordinates after the demi-tour.

These relations are used with simple ray tracing to obtain the phase space distributions after acceleration and after the demi-tour. The energy and time projections give the calculated energy and time spectra for comparison with the experimental spectra.

The initial phase space parameters at the injector cavity exit are determined by fitting the energy and time spectra for a range of RF phases. However, in practice, not all five parameters are varied to fit the data. At low-beam charge, and hence low-peak current, there are no pulse elongation effects in the injector cavity. Therefore, the electron beam pulse length, $\sqrt{\tau_{11}}$, is identical to the drive laser pulse length. In addition, the accelerator tuning procedure makes the injector cavity be phased such that a beam with minimum energy spread is produced after acceleration. Hence, it is a reasonably valid assumption that the energy spread is also a minimum at the injector cavity exit. This approximation leads to the waist conditions, $\tau_{12} = 0$. Therefore, the low-charge data is fit using only the three parameters : τ_{22} , a and b.

Discussion of the experimental results

This method of analysis has been applied to 1 nC per micropulse data with the results being given in figures 2 to 4. The best fit initial phase space parameters are :

$$\tau_{11} = 1600 \text{ ps}^2$$
$$\tau_{12} = 0 \text{ ps.MeV}$$
$$\tau_{22} = 2.5 \times 10^{-6} \text{ MeV}^2$$
$$a = 0 \text{ MeV/ps}^2$$
$$b = -1.10^{-6} \text{ MeV/ps}^3$$

As discussed in the previous section, $\sqrt{\tau_{11}}$ is determined by the drive laser pulse length and the initial ellipse is assumed to be at a waist in the beam energy, $\tau_{12} = 0$. The remaining three parameters have been varied to fit the electron energy spectra and the pulse lengths for a range of 433 MHz RF phase. It is interesting to note that the parabolic term, a, is not necessary to fit the data.

Figure 2a shows the initial and final phase spaces when the accelerator phase is adjusted for minimum energy spread, defined to be $\varnothing_{433} + 90°$. Figure 2b plots the experimental and calculated energy spectra for this phase and the level of agreement is seen to be excellent.

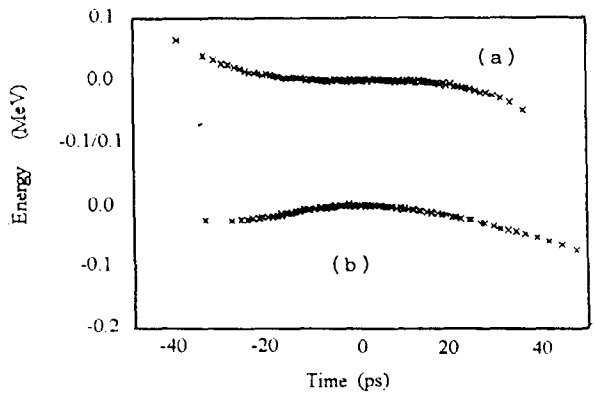

Fig. 2a Longitudinal phase spaces of the electron beam at the injector cavity exit (a) and after acceleration and transport around the non-isochronous demi-tour (b). The phase of the 433 MHz RF cavities is adjusted or minimum energy spread, $\varnothing_{433} = 90°$.

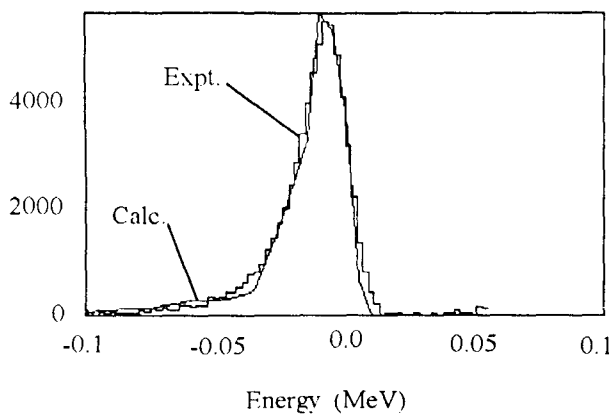

Fig. 2b Comparison of the experimental and fitted electron beam spectra. The fitted spectrum is calculated by performing the projection of the final phase space shown in Fig. 2a onto the energy axis.

Changing the 433 MHz RF phase by four degrees will bunch the beam as shown in Fig. 3. The energy spectrum exhibits the expected increase in energy spread with an interesting curved pattern for its phase space distribution. And again there is excellent agreement of the calculation with the experimental energy spectrum.

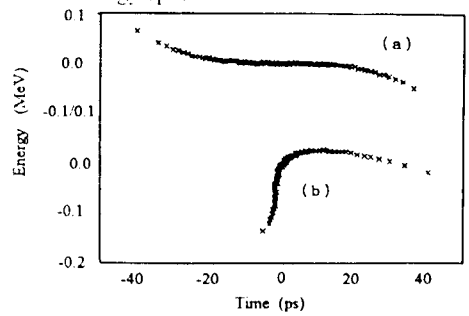

Fig. 3a Longitudinal phase spaces of the electron beam at the injector cavity exit (a) and after acceleration and transport around the non-isochronous demi-tour (b). The phase of the 433 MHz RF cavities is adjusted to bunch the beam, $\varnothing_{433} = 86°$.

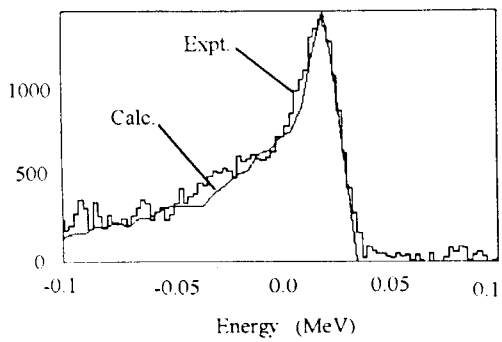

Fig 3b Comparison of the experimental and fitted electron beam spectra. The fitted spectrum is calculated by performing the projection of the final phase space shown in Fig. 3a onto the energy axis.

The electron beam pulse length after the demi-tour as a function of $\varnothing_{433}$ is plotted in Fig. 4, with the fit reproducing the data over the measured phase range.

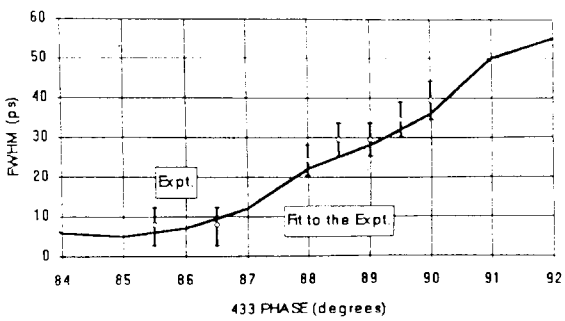

Fig. 4 Dependence of the electron beam pulse width upon the 433 MHz RF phase. The data has been corrected for the streak camera resolution, and the calculated fit is based on the initial phase space parameters given in the text. The electron beam pulse length has been compressed by a factor of eight in this experiment.

Transverse emittance measurements

Beam transverse emittance was measured at the end of the linac by means of the three-gradient technique. The beam is focused in both vertical and horizontal directions by using a triplet and scanned with the last one. Data are taken for 7 to 10 different values of the quadrupole current.

Because of radial and longitudinal space-charge effects, transverse emittance is strongly dependent upon the current of the anode coil located at the photo-injector exit. It has been investigated for three different bunch charges : 0.2, 1.0 and 2.0 nC.

The minimum vertical and horizontal emittances are plotted in Fig. 5 as a function of the bunch charge.

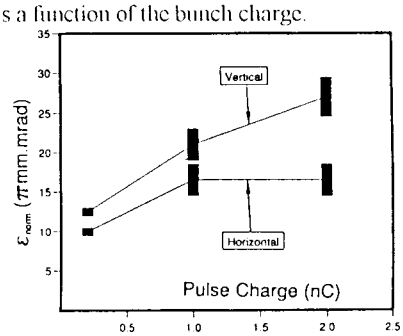

Fig. 5 Dependence of the normalized transverse emittances on the bunch charge.

The difference between horizontal and vertical emittances is probably due to alignment imperfections of the anode-coil in the photo-injector or to the drive laser incidence angle on the photocathode of ~ 60 degrees, causing a 10 ps delay across the laser spot and generating a non axisymmetric e-bunch.

Conclusions

We have developed a technique for analyzing electron beam energy and time spectra to obtain the longitudinal phase space distribution at the exit of a photocathode injector cavity. At 1 nC of micropulse charge, the data is well represented by a phase space ellipse distorted only with a cubic function. For this bunch charge and a peak current of 50 A, the emittances are :

$\varepsilon_x^{rms} = 4\ \pi.\text{mm.mrad}$

$\varepsilon_y^{rms} = 5.4\ \pi.\text{mm.mrad}$

$\varepsilon_l^{rms} = 0.063\ \pi.\text{ps.MeV}$

leading to a generalized beam brightness [2]

$B' = 0.75\ 10^{21}\ A/\pi^3.m^2.rad^2$

References

[1] D.H. Dowell et al., Nucl. Instr. Meth. A318(1990)447.

[2] S. Joly et al., Nucl. Instr. and Meth. A341(1994)386.

[3] A. Loulergue et al., "Transverse and longitudinal emittance measurements in the ELSA linac", Proc. of the EPAC-94 Conference, London, June 27-July 1rst, 1994, to be published.